Journal of Quantitative Spectroscopy & Radiative Transfer 262 (2021) 107500

Contents lists available at ScienceDirect

Journal of Quantitative Spectroscopy & Radiative Transfer

journal homepage: www.elsevier.com/locate/jqsrt

Exceptional adaptable MWIR thermal emission for ordinary objects covered with thin VO_2 film

Hasan Kocer[a,*], Mehmet Cihan Cakir[a], Yilmaz Durna[a], Mahmut Can Soydan[a,b], Oguz Odabasi[a,b], Halil Isik[a], Koray Aydın[e], Ekmel Özbay[a,b,c,d,*]

[a] NANOTAM-Nanotechnology Research Center, Bilkent University, 06800 Ankara, Turkey
[b] Department of Electrical and Electronics Engineering, Bilkent University, 06800 Ankara, Turkey
[c] Department of Physics, Bilkent University, 06800 Ankara, Turkey
[d] UNAM-Institute of Materials Science and Nanotechnology, Bilkent University, 06800 Ankara, Turkey
[e] Department of Electrical Engineering and Computer Science, Northwestern University, 60208 Evanston, IL, United States

ARTICLE INFO

Article history:
Received 25 September 2020
Revised 18 November 2020
Accepted 27 December 2020
Available online 20 January 2021

Keywords:
Thermal emission
Thermography
Thin film
Vanadium dioxide
Phase transition
Thermal camouflage

ABSTRACT

Monotonous thermal radiation emitted from an ordinary object can be brought into a dynamic and versatile form that can be shaped according to the application area with the ingenious design of the surface coatings. Building the coatings with phase change materials provides exceptional and surprising properties in terms of tunability, adaptability and multifunctionality. In this paper, we investigate the thermal radiation properties in the MWIR band through comprehensive thermographic measurements and theoretical methods while a thin (~90 nm thick) vanadium dioxide (VO_2) layer on the sapphire substrate (VO_2 thin film) is placed on different ordinary objects under heating/cooling conditions. It is indicated that the emission of the metal object (low emittance) can be boosted and the emission of the blackbody-like object (high emittance) can be suppressed at the relevant temperatures. The thermal emission of the objects covered with thin VO_2 film at high temperatures (>75 °C) is determined by only the VO_2 thin film, since the VO_2 layer is completely metallized and the MWIR radiation of the underlying object is masked. When the actual temperature of the object behaving like a blackbody rises up to 95 °C, the temperature detected in the MWIR thermal camera is reduced by more than 20% to approx. 75 °C due to the VO_2 thin film on this object, providing thermal camouflage. It is experimentally and theoretically revealed that the underlying physical mechanism on these strange results is associated with the drastic change in the infrared optical parameters of the VO_2 as a result of the applied temperature.

1. Introduction

There is great interest in thermal emission engineering for a wide range of applications, such as infrared (IR) invisibility/camouflage [1,2], energy harvesting [3,4], and IR radiation and heat management [5,6]. The thermal radiation or emission (TE) in the IR band emitted from the objects depends on the temperature and spectral emissivity of the object [7]. Since the spectral emissivity of conventional materials is between 0 and 1, depending on the material type and geometry, the TE of such materials is directly proportional to the temperature. In other words, the warmer the material, the higher the TE coming from the material. In addition, according to Kirchhoff's law, since the spectral emissivity is equal to spectral absorptivity [8], the higher the spectral emissivity at a certain wavelength emitted from the object, the higher the spectral absorptivity, which is the rate of absorption of the illumination at the same wavelength. When thin films are coated on the object to which TE control is desired, the spectral emissivity of the object can be controlled depending on the geometric pattern and material content of the film, and consequently TE can be engineered [5]. However, in most of these studies, thin films coated on the objects provide passive, that is, mono-functional properties of the spectral emissivity [6,9,10]. The most important constraint of passive coatings is that if a different spectral emissivity or absorptivity requirement occurs in the lifetime of the object and/or the ambient conditions in which it lives, complex, time-consuming, and costly design and fabrication processes need to be repeated according to the requirements [11,12].

If phase change material (PCM) is used in a thin-film design, the above-mentioned passivity and mono-functionality features can be changed in TE control without making a new design and fabrication, resulting in dynamism, adaptability, and

* Corresponding authors.
E-mail addresses: hasan.kocer@bilkent.edu.tr (H. Kocer), ozbay@bilkent.edu.tr (E. Özbay).

https://doi.org/10.1016/j.jqsrt.2020.107500
0022-4073/

multifunctionality. Germanium antimony telluride (GeSbTe or GST) chalcogenide [13], perovskite manganese oxide [14], tungsten oxide (WO_3) [15,16], samarium nickel oxide ($SmNiO_3$) [17], and most importantly vanadium dioxide (VO_2) [18–20] can be listed as prominent PCMs with TE studies [21]. The material phase of VO_2 changes reversibly when it exceeds an easily accessible temperature (~68 °C) level [22]. In other words, the material exhibits a controllable dynamic characteristic that is an insulator at room temperature, metal at high temperatures, and a mixture of both material components (i.e. natural metamaterial [23]) at intermediate temperatures. The phase transition of VO_2 can be performed thermally [24–27], optically [28], electrically [29–31], and mechanically [32]. The electrical and optical properties of VO_2 differ significantly, especially in the IR spectrum, depending on the insulating, conductive, and natural metamaterial states. As a result of this, by making use of the developing micro and nano fabrication possibilities, many optical and photonic applications that use insulator and metal conditions other than the phase transition region have been developed [25–27,33], and the door has been opened to benefit from the extraordinary behavior in the intermediate region [24,34]. This intermediate zone is the regime in which the material itself operates as a metamaterial in which subwavelength metallic and insulating inclusions change in size and pattern depending on the amplitude and the direction (i.e. heating and cooling) of the temperature during the phase transition. A comprehensive study of extracting the optical parameters of VO_2 during the phase transition can be found in our recent study [24].

In the present paper, we experimentally explore 3–5 μm mid-wave IR (MWIR) TE of the ordinary objects covered with a thin VO_2 film according to temperature variations of the underlying object under heating and cooling conditions. Although the thermal imaging applications are more in 8–14 μm long-wave IR (LWIR) band, the opacity of the sapphire substrate in this band interrupts the radiation of the objects under it. For this reason, we choose the MWIR band to better observe the interaction of the radiation of the underlying objects and the thin film radiation. Since the spectral optical parameters of the VO_2 film at different temperatures are dependent on the synthesis conditions (growth type, substrate, film thickness, etc.) [24,34,35], we experimentally reveal the optical properties of the film in the IR band based on the quantitative spectroscopy method in our previous study [24]. Next, MWIR TEs originating from two different ordinary objects covered with thin VO_2 film are measured in heating and cooling cycles by MWIR thermal microscopy and compared with calculations made with a radiative transfer model based on electromagnetic simulations. With the motivation to better observe and survey the effect of the thin film coating on the objects with different radiative properties, we choose two distinct objects: "Object 1″ is a blackbody-like with an emissivity close to 1, while "Object 2″ is a metal with near-zero emission. It is demonstrated by compatible measurements and theoretical calculations that the monotone radiation property of the uncoated objects can be transformed into a non-monotone form thanks to the extraordinary properties of VO_2 during phase transition when a very thin VO_2 coating is applied. Benefiting from these features, our study contributes to unlocking the multifunctional and adaptable thermal emission application potentials, such as thermal camouflage.

2. Materials and methods

2.1. Synthesis of thin VO_2 film

~90 nm thick thin VO_2 film was deposited on a double side polished *c*-plane sapphire substrate utilizing the RF magnetron sputtering technique. Sapphire was chosen as the substrate since it has superior transmittance up to 6 µm mid infrared wavelengths. We will refer to the structure of "90 nm thick thin VO_2 film on sapphire substrate" as "VO_2 thin film" throughout the present paper. The source material was taken as a vanadium oxide target. The deposition rate was ~0.4 A°/s under the deposition pressure of 2.4×10^{-3} mbar and argon (Ar) flow of 7 sccm. Post annealing was performed at 400 °C for 60 min in an atmospheric tube furnace under Ar flow of 4 cm^3/min.

2.2. Electrical characterization of VO_2 thin film

The DC electrical sheet resistance of VO_2 thin film was measured with the 4-probe sheet resistance technique (Agilent B1500A Semiconductor Parameter Analyzer) while changing the temperature from 25 °C to 90 °C and then back down. A thermoelectric cooling (TEC) chuck and its controller (10A/12 V TEC controller, Arroyo Instruments 5310) were used as the heating stage to control the temperature. At each temperature measurement, we waited at least 60 s for the temperature to settle. DC electrical sheet resistance measurements proved that the VO_2 thin film is a suitable PCM material with a reversible material phase by transitioning from the insulating state to the conductive state with a very steep slope with respect to the temperature change. (More than four orders of variation in the resistance value between cold (T = 25 °C) and hot (T = 90 °C) conditions).

2.3. Structural characterization of VO_2 thin film

The surface morphology/topography and surface roughness of VO_2 thin film were investigated using scanning electron microscopy (SEM) and atomic force microscopy (AFM). According to the SEM image, the surface morphology of the VO_2 film was continuous with multi domains due to the RF magnetron sputtering. In addition, the average surface roughness was found to be ~8 nm in the AFM imaging. This value of roughness is negligible compared to the wavelengths ($\lambda \geq 1$ μm) in our study. Therefore, in simulations of these wavelengths, it would be correct to consider the top of the VO_2 film as smooth.

2.4. Measurements

2.4.1. Fourier transform infrared spectrometer measurements

The temperature dependent IR spectral reflectivity of the VO_2 thin film was measured employing an IR microscope (Bruker Hyperion 2000) and the Fourier transform infrared (FTIR) spectrometer (Bruker Vertex 70v) with a liquid nitrogen cooled HgCdTe detector and mid-IR source. A 15x magnification reflective objective (numerical aperture: 0.4) was selected to collect the reflected light. For calibration in the reflectivity measurements, we utilized an optically thick gold layer coated on the sapphire substrate as the reference. VO_2 thin film was placed on a heating stage. With the heating stage mounted on the IR microscope and a temperature controller (Arrayo TEC), changes were performed from room temperature (T = 25 °C) to higher temperature (T = 90 °C) during heating and from T = 90 °C to T = 25 °C during cooling. After setting the controller of the heating stage, we took particular care to wait at least 60 s for the sample to reach the desired temperature.

2.4.2. Thermal microscopy measurements

IR thermographic measurements were carried out using a thermal microscope (QFI InfraScope TM-HST) operating at the MWIR spectrum with a liquid nitrogen cooled InSb detector array. The thermal microscope was in a laboratory environment that is not subject to extremes of heat or cold. 12x lens using the Lens Turret was selected in the measurements. For a blackbody-like object (Object 1), the thermal microscope's black calibration tool (emissivity of the object, ε_{object}=0.95) was used, while the metal chuck

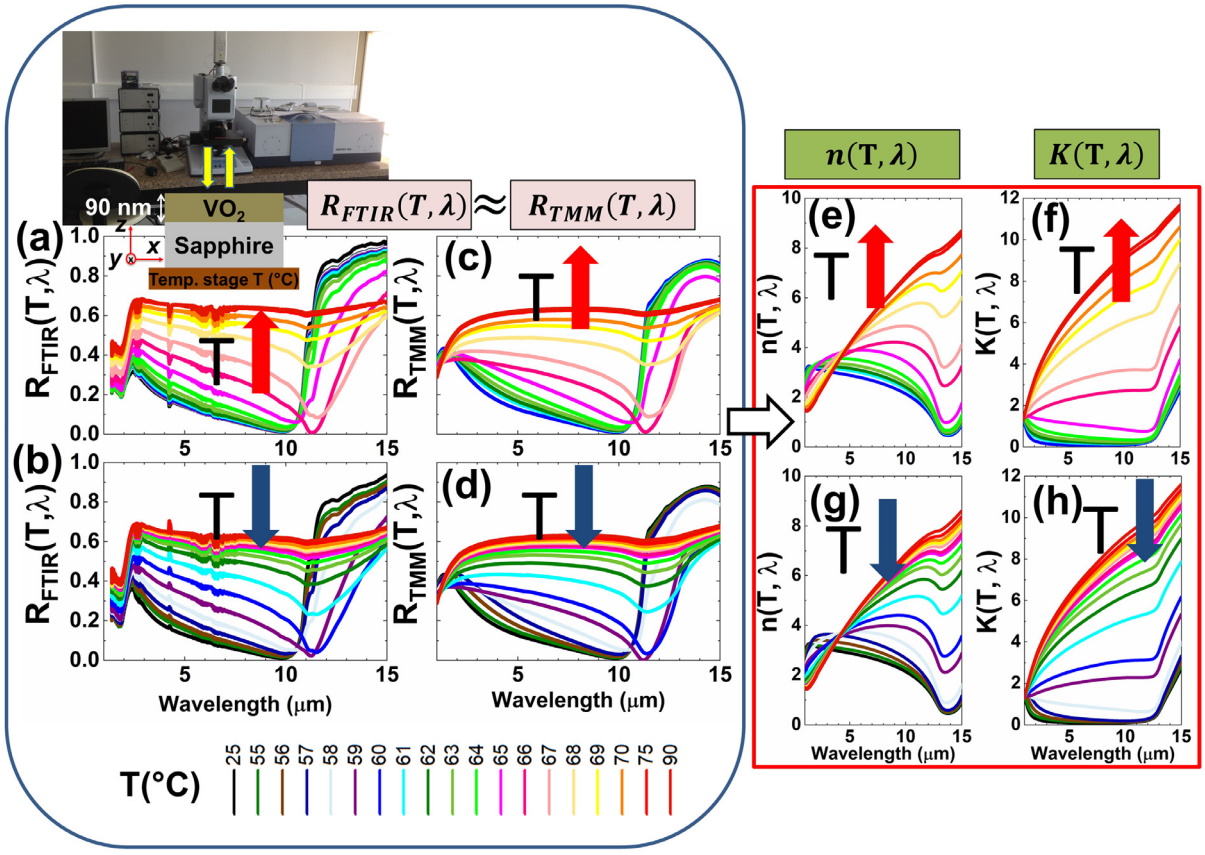

Fig. 1. Extraction method of spectral optical parameters of VO_2 with respect to temperature. Measured spectral reflectivity of R_{FTIR} (T, λ) (a) during heating and (b) during cooling. Simulated spectral reflectivity of R_{TMM} (T, λ) (c) during heating and (d) during cooling. Inset (a): FTIR measurement setup and x-z side view of the VO_2 thin film on a temperature stage. Extracted IR spectral optical parameters of VO_2 during heating: (e) Real and (f) imaginary parts of the refractive indices. Extracted IR spectral optical parameters of VO_2 during cooling: (g) Real and (h) imaginary parts of the refractive indices. The bottom colored vertical lines refer to the temperatures applied during heating and cooling.

of the thermal microscope (ε_{object}=0.20) was selected for low-emissivity metal (Object 2). Before starting the heating and cooling measurement cycles of the sample, we measured the internal IR background emission of the microscope system for calibration purposes. During this measurement, the system shuts itself off to the external IR radiation with a shutter. In order to obtain experimental average (band) emissivity of the objects covered with VO_2 thin film during heating and cooling cycles, the temperature of the metal chuck (temperature stage) of the thermal microscope was precisely changed from room temperature (25 °C) to 95 °C and vice versa with the QFI system software when the VO_2 thin film was placed on Object 1 and Object 2, respectively. At each temperature measurement, we waited at least 60 s for the sample to reach the desired temperature. Finally, a 2D surface temperature map of the VO_2 thin film on Object-1 was acquired while changing the stage temperature from low (50 °C) to high (95 °C) by setting the emissivity to a fixed value, which is selected as the emissivity value of the sample at 50 °C.

2.5. Simulations

2.5.1. Electromagnetic simulations

Electromagnetic simulations were performed with the transfer matrix method (TMM) to calculate the spectral transmittance $T(T, \lambda)$ and the spectral reflectivity $R(T, \lambda)$ of the VO_2 thin film. The spectral optical parameters of the 90 nm thick VO_2 layer, which we extracted according to the temperature [24], were used. The spectral optical parameter of the sapphire substrate was taken from the Palik database [36]. In the TMM method, the multilayer optical calculations can be achieved by cascading the layers in which the field within each layer could be treated as the superposition of a forward-traveling (transmitted) and backward-traveling (reflected) wave with a wave number and a transfer matrix that could represent the propagation through the interface or within the medium [37,38]. The mathematical details of these derivations for TMM were given by Kocer et al. [9]. In TMM simulations, we illuminated the VO_2 thin film at the normal incidence.

2.5.2. Heat transfer simulations

Details of the heat transfer mechanisms and the simulations are given in the Supplementary Material.

3. Results and discussions

3.1. Determination of the VO_2 dynamic optical parameters

Spectral optical parameters of VO_2 in the IR wavelengths are determined by the method shown in Fig. 1. This method, whose details were described in our previous study [24], is based on the convergence of the theoretical spectral reflectivity values ($R_{TMM}(T, \lambda)$) calculated with the TMM electromagnetic simulations to the experimental ones ($R_{FTIR}(T, \lambda)$) during heating and cooling cycles. The main reason why we make temperature changes separately for the heating and the cooling is that the hysteric effects on the optical parameters are revealed with the specified temperature cycles, as VO_2 has a certain hysteresis inherent in the material na-

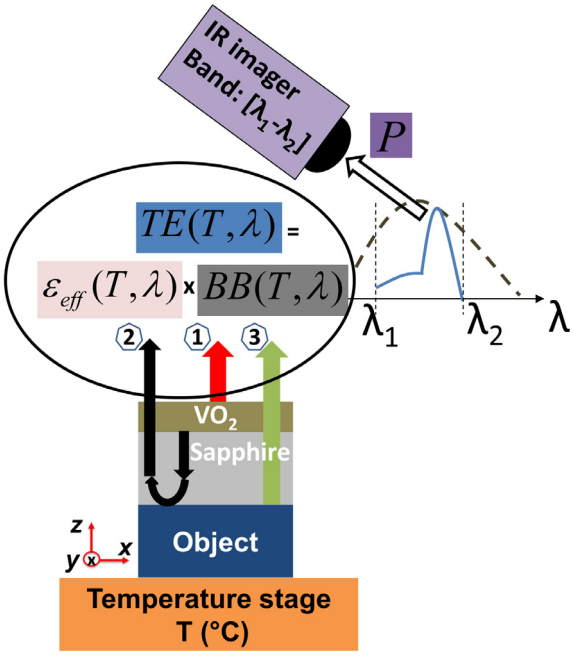

Fig. 2. Modeling of thermal emission.

ture [24,34,39] during the thermally driven transition from insulator to metal (or vice versa). The history of temperature profile (i.e., knowing VO_2 under heating or cooling path) should be tracked in order to manage the hysteresis of VO_2 in practical applications. Otherwise, the device needs to be "reset" every time before uses. The temperature-varying spectral optical parameters of the VO_2 layer for heating and cooling conditions in the temperature range T = 25–90 °C are modeled using an effective medium theory (EMT) in the electromagnetic TMM simulations. By fitting the tuning parameters in the EMT modeling elaborated in our past work [24], the spectral FTIR measurements during the heating (Fig. 1(a)) and the cooling (Fig. 1(b)) as well as the corresponding TMM simulations in Fig. 1(c) and Fig. 1(d) are matched in the range of 1–15 μm IR wavelengths. The corresponding temperatures are shown by colored vertical lines below the figure. Then, the extracted IR spectral optical parameters of VO_2 are given as real ($n(T, \lambda)$) and imaginary ($K(T, \lambda)$) parts of the refractive indices during heating ((Fig. 1(e) an Fig. 1(f)) and cooling ((Fig. 1(g) and Fig. 1(h)).

3.2. Modeling thermal emission from the objects covered with thin film coating

Using the dynamic optical properties of VO_2, we will model all thermal radiation processes reaching an IR imager from various ordinary objects coated with VO_2 thin film as shown in Fig. 2. The temperature dependent spectral thermal emission ($TE(T, \lambda)$) radiant from any object is generally expressed as [5,17,35,40]

$$TE(T,\ \lambda) = \varepsilon_{eff}(T,\ \lambda).BB(T,\ \lambda) \tag{1}$$

where $\varepsilon_{eff}(T, \lambda)$ is effective spectral emissivity, and $BB(T, \lambda)$ is the spectral emission of a blackbody (BB), which is also well known as Planck's law [41] and defined by

$$BB(T,\ \lambda) = \frac{2\pi hc^2}{\lambda^5\left(\exp\left(\frac{hc}{\lambda k_B T}\right) - 1\right)}. \tag{2}$$

Here h, k_B and c are all constant numbers, which are Planck's constant, Boltzmann's constant, and the speed of light in vacuum, respectively. When we combine the constant numbers in (5) and take the λ in micrometer (μm) and the T in Kelvin (K), it would be more convenient to reformulate $BB(T, \lambda)$ in W/(cm^2.µm) as

$$BB(T,\ \lambda) = \frac{c_1}{\lambda^5(\exp\left(c_2/\lambda T\right) - 1)} \tag{3}$$

where c_1=3.7418 × 10^4 W.cm^{-2}.µm^4 and c_2=1.4388 × 10^4 µm.K. As shown in Fig. 2, if there was no thin film coating on any ordinary object (blue colored), the emitted $TE(T, \lambda)$ function of the object would be equal to the product of ε_{object} and $BB(T, \lambda)$ function. For ordinary (uncoated) objects, $\varepsilon_{eff}(T, \lambda)$=$\varepsilon_{object}$ which is a constant number in the 0–1 interval (i.e. ε_{object} is a fixed value close to zero for metallic objects whereas ε_{object} is a fixed value close to 1 for blackbody-like objects). Then, $TE(T, \lambda)|_{\text{ordinary obj.}}$=$\varepsilon_{object}$.$BB(T, \lambda)$. In other words, the spectral behavior of the $TE(T, \lambda)$ function of the ordinary objects with respect to the wavelength will, as expected, be similar to the function $BB(T, \lambda)$ shown by the black dashed spectral curve in the figure. When the temperature of the ordinary object increases, while the emissivity remains constant, the blackbody function increases, and as a result, the thermal emission increases. This usual radiation characteristic can be transformed into a variety of non-monotonous forms thanks to a very thin film coating on the object, shown by the solid blue spectral curve as an example in the figure.

When thin film is coated on the object, the emissivity $\varepsilon_{eff}(T, \lambda)$ of the "film+object" can vary with temperature and/or wavelength depending on the film properties (geometry, material components) and interaction with the object. As a result, the usual attitude of the thermal emission can be deliberately extraordinary.

In the figure above, we will model the situation when the planar VO_2 thin film (90 nm thick VO_2 layer on the sapphire substrate) is coated on the object. However, the approach here applies to any thin film structure on any object, regardless of whether the film is structured or planar. The $\varepsilon_{eff}(T, \lambda)$ of the "VO_2 thin film+object" can be modeled as $\varepsilon_{eff}(T,\ \lambda) = \sum_{j=1}^{3} \varepsilon_j(T,\ \lambda)$ according to its components, which are schematized with numbers labeled in the figure and expressed below [40].

Spectral emissivity contribution of VO_2 thin film in the forward direction labeled "1" (red colored) in the figure as

$$\varepsilon_1(T,\ \lambda) = \varepsilon_{VO_2}(T,\ \lambda) = 1 - R_{VO_2}(T,\ \lambda) - T_{VO_2}(T,\ \lambda) \tag{4a}$$

where $R_{VO2}(T, \lambda)$ and $T_{VO2}(T, \lambda)$ are the spectral reflectivity and the transmissivity of the VO_2 thin film, respectively. Note that we also apply Kirchhoff's law here that $\varepsilon_{VO2}(T, \lambda)$=$A_{VO2}(T, \lambda)$ where $A_{VO2}(T, \lambda)$ is the spectral absorptivity.

Spectral emissivity contribution of VO_2 thin film in the backward direction labeled "2" (black colored) in the figure as

$$\varepsilon_2(T,\ \lambda) = \left(1 - \varepsilon_{object}\right).T_{VO_2}(T,\ \lambda).\varepsilon_{VO_2}(T,\ \lambda). \tag{4b}$$

Here, the reverse radiation from the VO_2 thin film to the object direction will be reflected back by multiplying the reflectivity of the object and then transmitted by the VO_2 thin film itself in the forward direction by multiplying the spectral transmissivity of the film. We assume that the object is opaque and then the reflectivity of the object can be determined by 1-A_{object}=1-ε_{object}.

Spectral emissivity contribution of the object in the forward direction labeled "3" (green colored) in the figure as

$$\varepsilon_3(T,\ \lambda) = T_{VO_2}(T,\ \lambda).\varepsilon_{object}. \tag{4c}$$

With this last term, it is clearly seen that the radiation emitted from the object is modulated by the spectral transmissivity of the VO_2 thin film as it travels forward through the film.

Optical power density (P/A) perceived in the far field in an IR imager operating between the wavelengths λ_1 and λ_2 can be calculated by integrating the spectral thermal emission in the

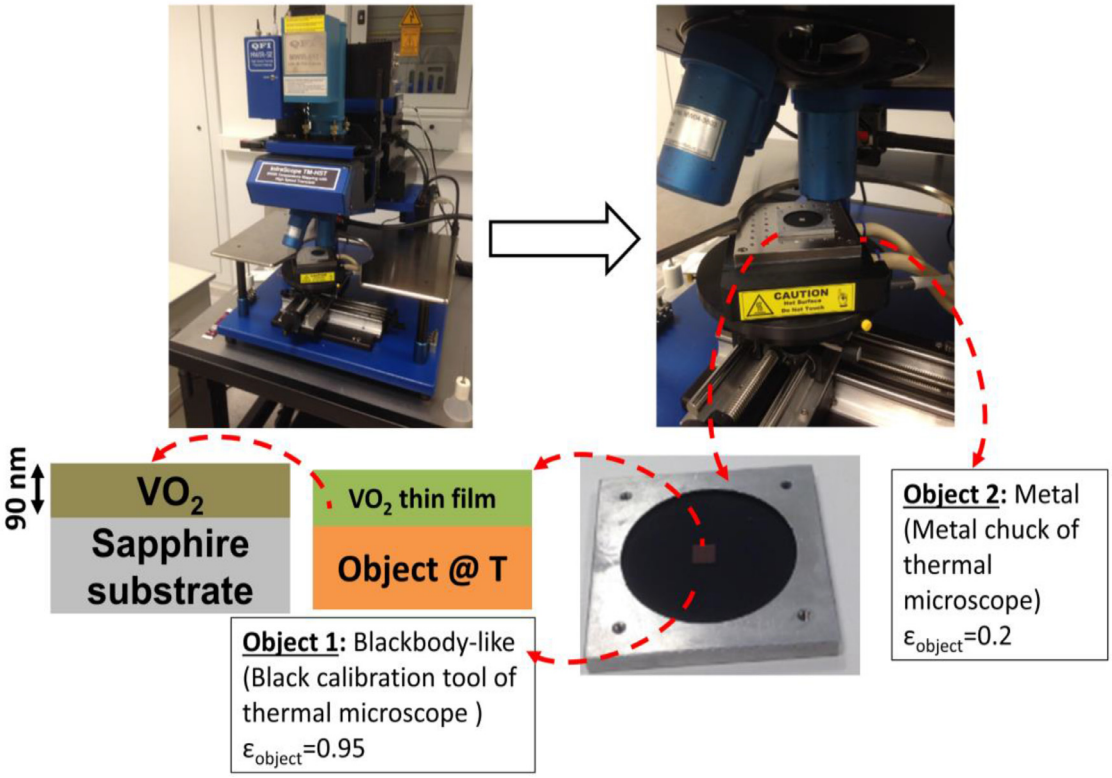

Fig. 3. Experimental setup for thermal emission.

operating wavelength range as follows

$$\frac{P}{A} = \int_{\lambda_1}^{\lambda_2} TE(T, \lambda).d\lambda \tag{5}$$

where P is the optical power and A is the sensor area of the IR imager. In this calculation, the atmosphere (the medium between the coated object and the IR imager) is considered to be transparent to the thermal radiation within the spectral range of interest.

Finally, the optical power from the sample integrated on the IR imager wavelength range in (5) can be normalized with respect to the reference perfect blackbody radiation on the same imager. In this way, we can compute the average (band) emissivity given by

$$\langle \varepsilon \rangle = \frac{\int_{\lambda_1}^{\lambda_2} TE(T, \lambda).d\lambda}{\int_{\lambda_1}^{\lambda_2} BB(T, \lambda).d\lambda}. \tag{6}$$

3.3. Measurement and simulation results

The thermal emission measurement setup is shown in Fig. 3. We utilize an MWIR thermal microscope (QFI InfraScope TM-HST), where the details about the measurement system are specified in the materials and methods section. The main purpose of our measurement in the 3–5 μm MWIR band is to examine the optical interaction with the objects under the VO_2 thin film in detail, since the sapphire substrate underlying the VO_2 layer is transparent in this band. We select two different objects with extreme object emissivities to represent a wide variety of ordinary objects that exist in nature, and we perform thermal microscopy measurements while the VO_2 thin film is on these objects. Accordingly, as shown in the figure, the black calibration tool (ε_{object}=0.95) of the thermal microscope is used for the high emissivity (blackbody-like) object (Object 1), while the metal chuck (heating stage) of the thermal microscope (ε_{object}=0.20) is employed for the low emissivity (metal) object (Object 2).

The measurement and simulation results of the average (band) emissivities in the MWIR spectrum are shown in Fig. 4 as the temperature increases (heating: $T\uparrow$ from 25 °C to 90 °C) and decreases (cooling: $T\downarrow$ from 90 °C to 25 °C) while the VO_2 thin film is on two different objects.

When the VO_2 thin film is on the blackbody-like object (Fig. 4(a)) and metal object (Fig. 4(c)), the experimental band emissivities are acquired during the heating and cooling by thermal microscopy described in the materials and methods section. In the simulation part, TMM electromagnetic simulations are carried out for the VO_2 thin film geometry (90 nm thick VO_2 on the sapphire substrate) under the normal incidence of MWIR wavelengths. The optical parameters of VO_2 at MWIR spectrum are taken from Fig. 1(e) to Fig. 1(h) at the respective heating/cooling temperatures. Since the sapphire is lossless in the MWIR, the refractive index in the electromagnetic simulations here is set to a constant 1.70 [27]. Then, the spectral reflectivity and transmissivity of the VO_2 thin film, $R_{VO2}(T, \lambda)$ and $T_{VO2}(T, \lambda)$, are found. Next, the spectral emissivity contributions modeled in (4a)-(4c) are computed. Finally, the simulated average emissivities are obtained with the help of (9) when the VO_2 thin film is on the Object 1 (Fig. 4(b)) and on the Object 2 (Fig. 4(d)). We have a pretty good agreement between the simulations and the measurements. The minor discrepancies between them are due to the imperfect experimental conditions. Looking at these experimental and simulation findings carefully, we can elucidate the following observations and evaluations: **(i)** Thanks to the thin VO_2 layer (~λ/45), the MWIR radiation characteristic of the ordinary objects under the film is engineered in an unusual way. **(ii)** Owing to the interaction with the thin film placed on Object 1, which behaves close to the blackbody without the film and has a high average emissivity of 0.95, the average emissivity in the MWIR band decreases by about 50% as the temperature rises. That is, the average emissivity, which is 0.8 at room temperature, decreases to 0.4 at T = 90 °C (Fig. 4(a) and Fig. 4(b)).

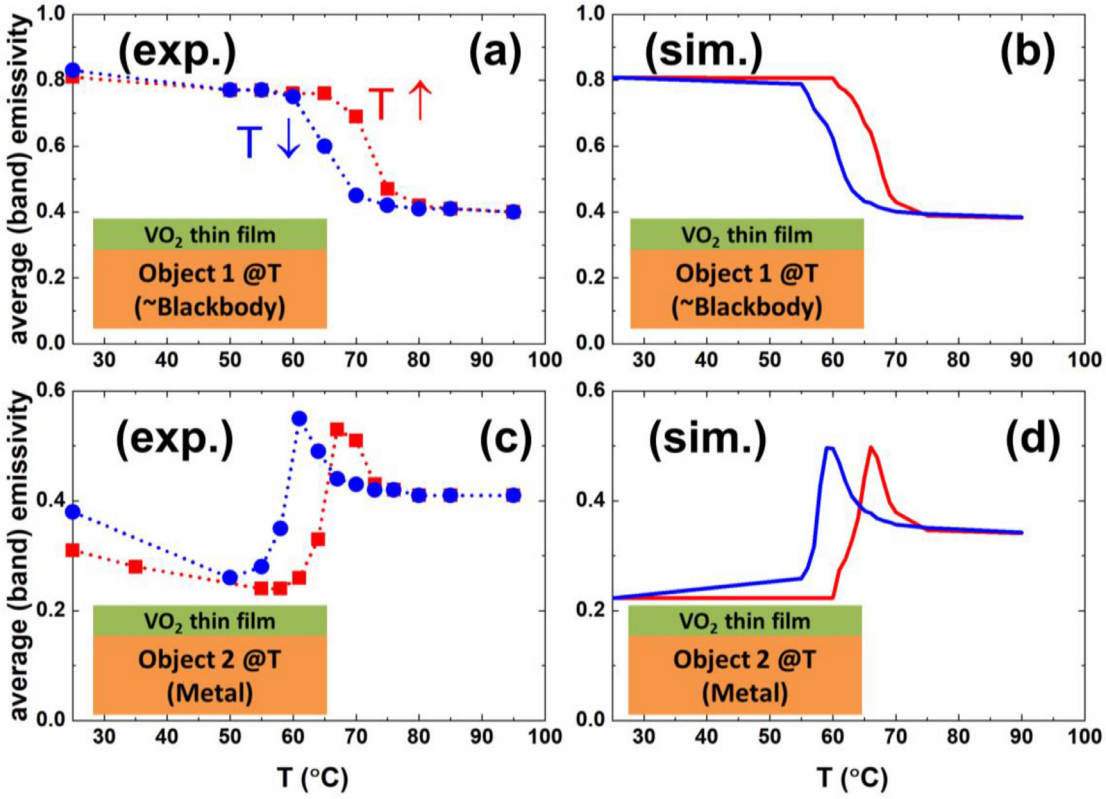

Fig. 4. Average (band) emissivity in MWIR for two different objects. (a) Experimental and (b) simulated average emissivity when the VO_2 film is on the blackbody-like object. (c) Experimental and (d) simulated average emissivity when the VO_2 film is on the metal object.

In addition, this falling rate occurs with a steep slope in the phase transition region of VO_2. **(iii)** The average emissivity of the coated Object 2 in the MWIR band exceeds the bare Object 2 value of 0.20 as the temperature rises due to the natural metamaterial behavior of the VO_2 during the phase transition (Fig. 4(c) and Fig. 4(d)). **(iv)** In the case of both objects, the inherent hysteric behavior of VO_2 happens between heating (red curves) and cooling (blue curves), especially at the phase transition temperatures. **(v)** At temperatures above about 75-80°, where VO_2 is all metal, the same average emissivity (~ 0.4) is obtained regardless of whether the object under the VO_2 thin film is like a blackbody or a metal. Since the VO_2 layer is completely metallized at the aforementioned temperatures, the MWIR radiation of the underlying object cannot be transmitted, so the average emissivity of the system turns into a state that can only be determined by the emissivity of the VO_2 thin film, regardless of the underlying object.

To better figure out the physical causes behind the temperature-dependent changes in the average emissivity mentioned above, we perform additional theoretical calculations with the TMM electromagnetic simulations as shown in Fig. 5 and Fig. 6. In Fig. 5, as a result of these TMM electromagnetic simulations, the spectral reflectivity, transmissivity, and absorptivity of the VO_2 thin film alone without an object underneath are exhibited in 3D plots to better visualize the impacts of the alterations in the wavelength and the temperature. In the spectral graphs during heating (Fig. 5(a)-Fig. 5(c)), at low temperatures, VO_2 is an insulator and, therefore, $R_{VO2}(T, \lambda)$ is low and $T_{VO2}(T, \lambda)$ is high as expected. With the onset of the phase transition of VO_2 from insulator to metal due to the temperature increase, $R_{VO2}(T, \lambda)$ rises rapidly and $T_{VO2}(T, \lambda)$ decreases abruptly. The spectral absorptivity, which is equal to spectral emissivity, can easily be computed by (4a) as discussed earlier. Given in Fig. 5(c), the relatively faint absorptivity value at low temperatures enhances with a steep slope at intermediate transition temperatures and finally saturates to a relatively larger value at higher temperatures. Conversely, while the temperature drops from 90 °C to 25 °C (cooling), as shown in Fig. 5(d)-Fig. 5(f), the opposite of the above events during the heating takes place with a certain hysteresis in the transition zone. As a common feature for all graphs, it is possible to claim that the spectral change of the parameters at a constant temperature is gradual rather than sudden changes with respect to the temperature at any fixed wavelength in the MWIR.

As visualized in Fig. 6, we can estimate the temperature and wavelength dependent effective spectral emissivity $\varepsilon_{eff}(T, \lambda) = \sum_{j=1}^{3} \varepsilon_j(T, \lambda)$ during the heating and cooling periods, when different objects are placed under the film whose 3D spectral properties are detailed above. Consistent with our experimental and simulation findings regarding the band emissivity explained previously (Fig. 4), we can shed light here on the following points: **(i)** Since the transparency, $T_{VO2}(T, \lambda)$, of the VO_2 thin film is much higher at low temperatures when the VO_2 layer is insulator (seen in Fig. 5(b) and Fig. 5(e)), the $\varepsilon_{eff}(T, \lambda)$ is determined by the emissivity of the underlying object regardless of the temperature direction. That is, $\varepsilon_{eff}(T, \lambda) \approx \varepsilon_3(T, \lambda) = T_{VO_2}(T, \lambda).\varepsilon_{object}$. **(ii)** At temperatures above 75–80°, where VO_2 is all metal $T_{VO2}(T, \lambda)$, is very low, so the underlying object's radiation is masked, and only $\varepsilon_{VO2}(T, \lambda)$ (in Fig. 5(c) and Fig. 5(f)) determines the $\varepsilon_{eff}(T, \lambda)$. **(iii)** At the intermediate temperatures where VO_2 is a mixed material, different effects occur according to the objects. In the case of a blackbody-like object (Fig. 6(a) and Fig. 6(b)), the impact of the high emissivity of the object, which dominates in the lower temperatures, gradually disappears as the temperature rises. However, the metal object reflects backward radiation from the VO_2 thin film, which rises with increasing temperature, in the forward direction as long as the thin film has transparency due to the mirror-like effect of the metal object, causing the effective emissivity to increase in the transition

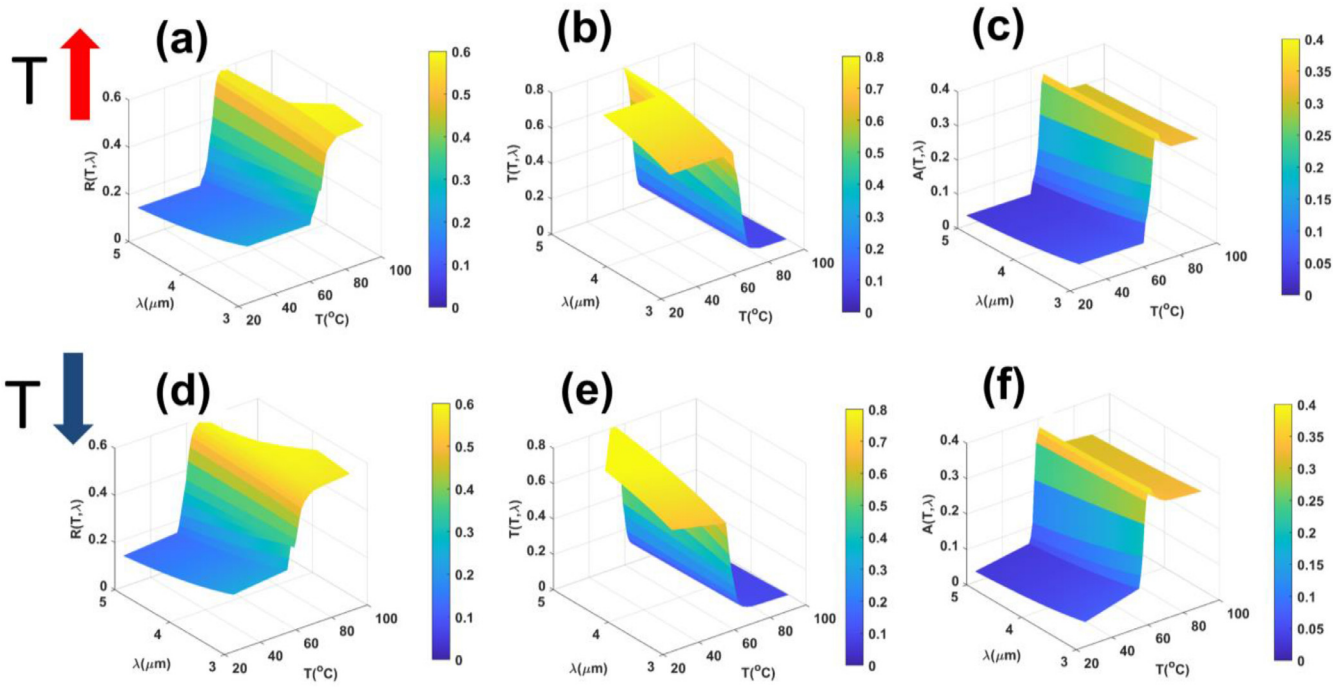

Fig. 5. Spectral characteristics of VO_2 thin film (90 nm VO_2 on sapphire) with respect to temperature. During heating: (a) Spectral reflectivity $R_{VO2}(T, \lambda)$, (b) spectral transmissivity $T_{VO2}(T, \lambda)$ and (c) spectral absorptivity $A_{VO2}(T, \lambda)$. During cooling: (d) Spectral reflectivity $R_{VO2}(T, \lambda)$, (e) spectral transmissivity $T_{VO2}(T, \lambda)$, and (f) spectral absorptivity $A_{VO2}(T, \lambda)$.

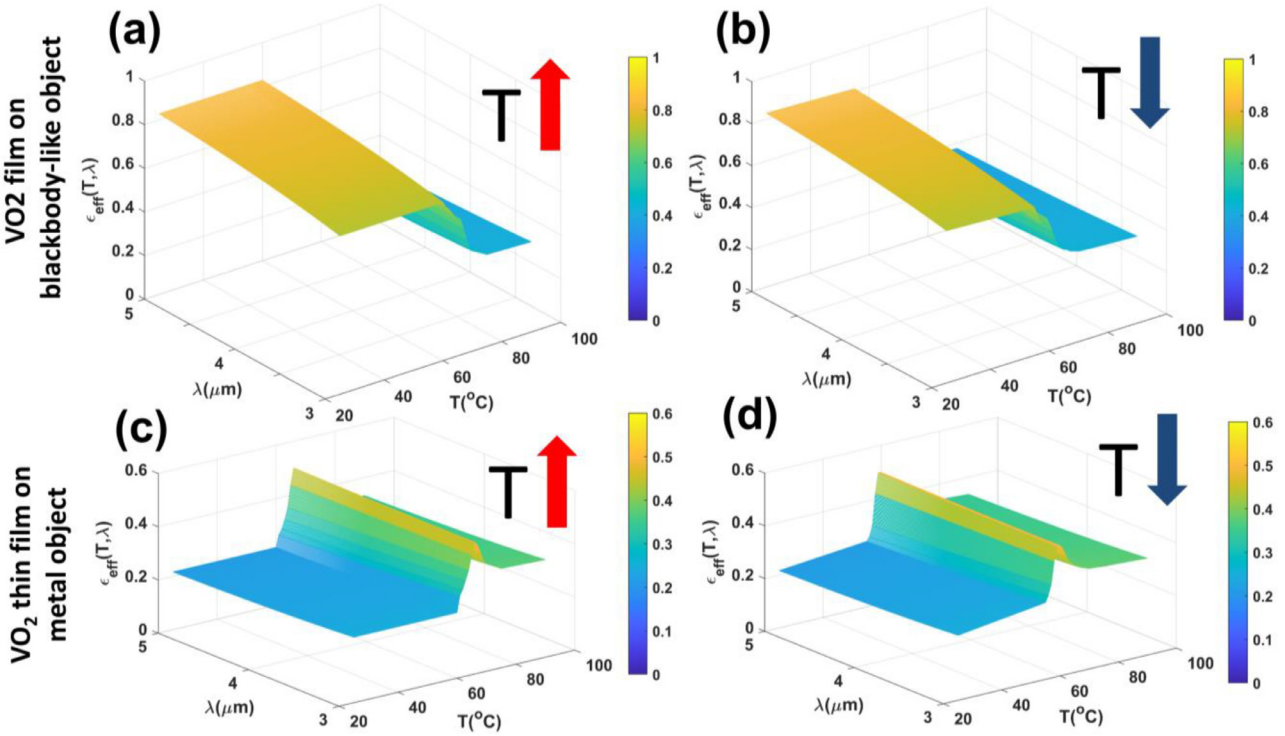

Fig. 6. Effective spectral emissivity ($\varepsilon_{eff}(T, \lambda)$) characteristics with respect to temperature. $\varepsilon_{eff}(T, \lambda)$ of VO_2 film on the blackbody-like object during (a) heating and (b) cooling. $\varepsilon_{eff}(T, \lambda)$ of VO_2 film on the metal object during (c) heating and (d) cooling.

region (Fig. 6(c) and Fig. 6(d)). In other words, the low IR radiation of the metal object is boosted at certain temperatures by the phase transition of VO_2. **(iv)** In the case of both objects, the aforementioned natural hysteric behavior of VO_2 is observed in all graphs, particularly at the phase transition temperatures.

To highlight the impact of the VO_2 thin film on the surface temperature measured by IR methods, we conduct additional experimental studies as shown in Fig. 7 and Fig. S2. In Fig. 7(a), we place the sample on the object (Object 1) that behaves like a blackbody. The 5 mm x 5 mm sample shown in Fig. 7(b) is essentially VO_2 thin film (90 nm VO_2 on the sapphire substrate). Utilizing electron beam evaporation, 150 nm thick gold (Au) is deposited on this sample in some places that appear yellow. With the 12x lens of the thermal microscope, we focus on the 1 mm x 1 mm

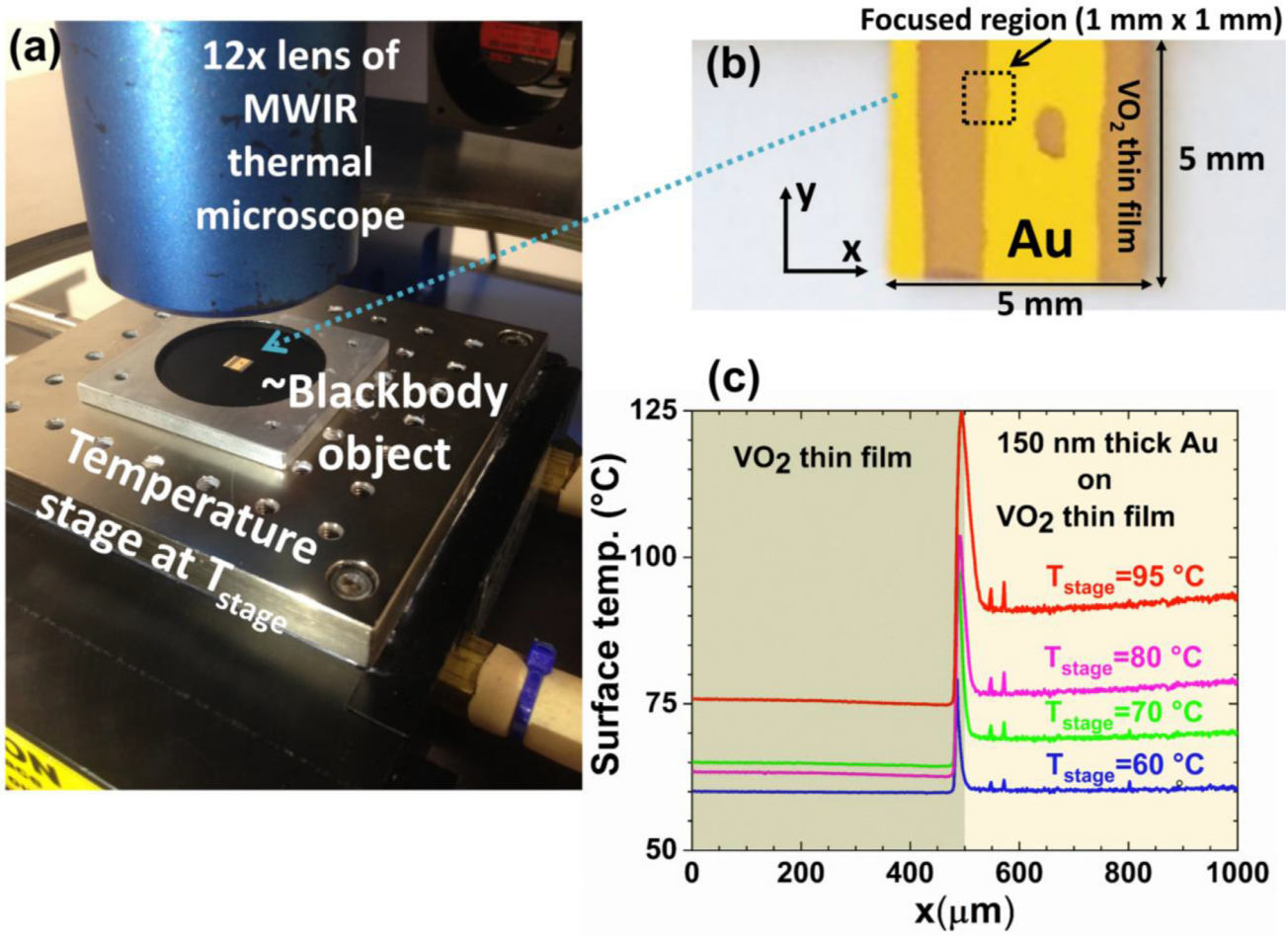

Fig. 7. Surface temperature measurements with respect to increasing stage temperatures (T_{stage}). (a) Measurement setup where the sample is on the blackbody-like object, (b) *x-y* view of the sample where the yellow regions are 150 nm thick Au coated on the VO_2 thin film and the black dotted square is the focus area under the thermal microscope and (c) Measured 1D surface temperatures with respect to *x* at constant mid *y* value in the focused region as the T_{stage} increases.

square (the black dotted area in Fig. 7(b)) and obtain the surface temperature map of this region via the thermal microscope in the MWIR band while the temperature of the heating stage (T_{stage}) is changed from low (50 °C) to high (95 °C). In the thermal microscope system, we fix the emissivity value of the sample to the value measured at T_{stage}=50 °C for subsequent temperature measurements at T_{stage}=60 °C, 70 °C, 80 °C, and 95 °C. The location that we choose for the area of focus is of particular importance. In this way, as shown in Fig. 7(b), the focused region at this location exhibits the characteristic that the left half is the VO_2 thin film and the right half is the optically thick (150 nm) Au on the film. While the emissivity of the optically thick gold-coated portion does not vary significantly in the temperature range, the behavior of the VO_2 thin film on Object 1 does change appreciably as revealed previously. Therefore, we will be able to experimentally demonstrate how two different surfaces on the same object, one with constant emissivity (optically thick Au on the VO_2 thin film) and the other with the emissivity varying with temperature (VO_2 thin film), can change the actual temperature of the object on their surface with thermographic temperature measurements in the MWIR band. The temperature maps obtained in this context are shown in Fig. 7(c) and Fig. S2. Note that the surface temperature refers to the temperature measured or detected in the MWIR thermal microscope, while the stage temperature refers to the actual temperature (See Supplementary Material for details).

Fig. 7(c) shows the 1D surface temperatures with respect to *x* at constant mid *y* value in the focused region as the T_{stage} increases. Here, it is clearly seen that as the T_{stage} rises, the surface temperature measured from the Au part increases at almost the same values of T_{stage}, while an extraordinary character is exhibited due to the VO_2 in the surface temperature measured from the VO_2 thin film. Initially, when the VO_2 is an insulator at T_{stage}= 60 °C, there is almost no temperature difference (i.e. ΔT=T_{stage}-$T_{surface}$), but after VO_2 is heated beyond the critical phase transition temperature (~68 °C), the ΔT increases significantly as VO_2 begins to transform from insulator to metal. Therefore, when the VO_2 is completely metal at T_{stage} = 95 °C, it is experimentally shown that the $T_{surface}$ detected by the MWIR thermal microscope is lowered as much as about 20°, i.e. $T_{surface}$~75 °C. The sudden and large jumps in surface temperature at the boundary line where two different regions meet (at x = 500 μm) may be originating from the loss of measurement performance due to edge effect in the thermal microscopy. In addition, relatively smaller temperature jumps around x = 550–600 μm can be called edge effects due to the roughness of the gold surface. Overall, with this experimental method, we can successfully compare quantitatively and visually how the surfaces mentioned above affect the thermographic temperature of a blackbody-like object, except for a few boundary lines where the edge effects occur.

The surface temperature character of the focused area, measured along the *x* and *y* axis, is also indicated in 3D in the Sup-

plementary Material (Fig. S2). Similar results, which we mentioned in the 1D graph above, are once again highlighted with 3D graphics, and when the temperature of the object behaving like a black body increases, the perceived temperature of the MWIR thermal camera decreases thanks to the VO_2 coated surface. In other words, thermal camouflage is experimentally demonstrated in the MWIR band.

Finally, we perform heat transfer simulations in the Supplementary Material (Fig. S1) for the bare substrate (sapphire) of the VO_2 thin film placed on Object 1 and Object 2, respectively. In the light of our findings, we see that the heater temperature is transmitted to the interface where the VO_2 is located with negligible losses. Therefore, it is possible to safely claim that the heater temperature levels (25 °C-95 °C) that we employed in our theoretical and experimental work above are felt at almost the same values in the topmost VO_2 layer regardless of the type of the object below.

4. Conclusions

In conclusion, through comprehensive experimental and theoretical methods, we investigated how a thin film containing VO_2 coated on the ordinary objects can reconstruct the thermal emission of these objects in a dynamic and reversible style. Utilizing the experimentally extracted dynamic optical properties of VO_2, we have developed a generic model with a TMM electromagnetic simulation support for all thermal radiation processes reaching the IR imager from various ordinary objects covered with VO_2 thin film. We selected two different ordinary objects (blackbody-like and metal) representing the emission range of ordinary objects and made MWIR thermal microscopy measurements while the VO_2 thin film was on them, applying temperature heating/cooling cycles in the range of 25 °C-95 °C. We showed that the MWIR thermal emission of ordinary objects under the film is unusually engineered by the interaction with the VO_2 thin film placed on these objects. Our experiments and simulations have clarified that the main factor of this extraordinary effect is the phase change of VO_2 with the applied temperature and, as a result, a drastic variation in its infrared optical parameters. With this bizarre interaction, and contrary to common sense, we have revealed that the emission of the low emittance object (metal) can be enhanced and the emission of the high emittance object (blackbody-like) can be diminished at the relevant temperatures. We also showed that thermal emission of the objects covered with thin VO_2 film at high temperatures (>75 °C) is determined by only the VO_2 thin film since the VO_2 layer is completely metallized and the MWIR radiation of the underlying object is masked.

The thermal camouflage was experimentally demonstrated through thermographically measured 1D and 3D temperature maps in such a way that when the actual temperature of the object behaving like a blackbody raised up to 95 °C, the temperature detected in the MWIR thermal camera was reduced by more than 20% to about 75 °C due to the VO_2 thin film on this object.

With the theoretical and experimental approach in our study, the usual thermal radiation of objects can be engineered into extraordinary dynamic and adaptive properties that have application potentials in various fields, such as thermal camouflage, sensors, etc., by designing structures in different geometries and patterns containing VO_2.

Declaration of Competing Interest

The authors declare that they have no known competing financial interests or personal relationships that could have appeared to influence the work reported in this paper.

CRediT authorship contribution statement

Hasan Kocer: Conceptualization, Methodology, Formal analysis, Investigation, Software, Data curation, Visualization, Writing - original draft, Writing - review & editing. **Mehmet Cihan Cakir:** Conceptualization, Methodology, Investigation, Data curation, Visualization, Writing - review & editing. **Yilmaz Durna:** Methodology, Software, Data curation, Visualization, Writing - review & editing. **Mahmut Can Soydan:** Methodology, Data curation, Visualization, Writing - review & editing. **Oguz Odabasi:** Methodology, Data curation, Visualization, Writing - review & editing. **Halil Isik:** Methodology, Software, Data curation, Visualization, Writing - review & editing. **Koray Aydın:** Conceptualization, Methodology, Writing - review & editing. **Ekmel Özbay:** Conceptualization, Methodology, Writing - review & editing, Supervision.

Acknowledgements

E. Ozbay acknowledges partial support from the Turkish Academy of Sciences (TUBA). K. Aydin acknowledges support from the Office of Naval Research Young Investigator Program (ONR-YIP) Award (N00014–17–1–2425).

Supplementary materials

Supplementary material associated with this article can be found, in the online version, at doi:10.1016/j.jqsrt.2020.107500.

References

[1] Kim T, Bae JY, Lee N, Cho HH. Hierarchical Metamaterials for Multispectral Camouflage of Infrared and Microwaves. Adv Funct Mater 2019;29:1–8. doi:10.1002/adfm.201807319.
[2] Xiao L, Ma H, Liu J, Zhao W, Jia Y, Zhao Q, et al. Fast Adaptive Thermal Camouflage Based on Flexible VO2/Graphene/CNT Thin Films. Nano Lett 2015;15:8365–70. doi:10.1021/acs.nanolett.5b04090.
[3] Zhou Z, Sakr E, Sun Y, Bermel P. Solar thermophotovoltaics: reshaping the solar spectrum. Nanophotonics 2016;5:1–21. doi:10.1515/nanoph-2016-0011.
[4] Bierman DM, Lenert A, Chan WR, Bhatia B, Celanović I, Soljačić M, et al. Enhanced photovoltaic energy conversion using thermally based spectral shaping. Nat Energy 2016;1. doi:10.1038/nenergy.2016.68.
[5] Baranov DG, Xiao Y, Nechepurenko IA, Krasnok A, Alù A, Kats MA. Nanophotonic engineering of far-field thermal emitters. Nat Mater 2019;18:920–30. doi:10.1038/s41563-019-0363-y.
[6] Peng L, Liu D, Cheng H, Zhou S, Zu M. A Multilayer Film Based Selective Thermal Emitter for Infrared Stealth Technology. Adv Opt Mater 2018;6:1–8. doi:10.1002/adom.201801006.
[7] Howell JR, Siegel R, Mengüç MP. Thermal radiation heat transfer. 6th ed. CRC Press; 2016.
[8] Xiao Y, Wan C, Shahsafi A, Salman J, Yu Z, Wambold R, et al. Precision Measurements of Temperature-Dependent and Nonequilibrium Thermal Emitters. Laser Photon Rev 2020 1900443:1900443. doi:10.1002/lpor.201900443.
[9] Kocer H, Butun S, Li Z, Aydin K. Reduced near-infrared absorption using ultrathin lossy metals in Fabry-Perot cavities. Sci Rep 2015;5:1–6. doi:10.1038/srep08157.
[10] Yildirim DU, Ghobadi A, Soydan MC, Atesal O, Toprak A, Caliskan MD, et al. Disordered and Densely Packed ITO Nanorods as an Excellent Lithography-Free Optical Solar Reflector Metasurface. ACS Photonics 2019;6:1812–22. doi:10.1021/acsphotonics.9b00636.
[11] Hail CU, Michel AKU, Poulikakos D, Eghlidi H. Optical Metasurfaces: evolving from Passive to Adaptive. Adv Opt Mater 2019;7:1–29. doi:10.1002/adom.201801786.
[12] Hajian H, Ghobadi A, Butun B, Ozbay E. Active metamaterial nearly perfect light absorbers: a review [Invited]. J Opt Soc Am B 2019. doi:10.1364/josab.36.00f131.
[13] Tittl A, Michel AKU, Schäferling M, Yin X, Gholipour B, Cui L, et al. A Switchable Mid-Infrared Plasmonic Perfect Absorber with Multispectral Thermal Imaging Capability. Adv Mater 2015;27:4597–603. doi:10.1002/adma.201502023.
[14] Fan D, Li Q, Xuan Y, Tan H, Fang J. Temperature-dependent infrared properties of Ca doped (La,Sr)MnO 3 compositions with potential thermal control application. Appl Therm Eng 2013;51:255–61. doi:10.1016/j.applthermaleng.2012.07.046.
[15] Franke EB, Trimble CL, Hale JS, Schubert M, Woollam JA. Infrared switching electrochromic devices based on tungsten oxide. J Appl Phys 2000;88:5777–84. doi:10.1063/1.1319325.

[16] Demiryont H, Moorehead D. Electrochromic emissivity modulator for spacecraft thermal management. Sol Energy Mater Sol Cells 2009;93:2075–8. doi:10.1016/j.solmat.2009.02.025.
[17] Shahsafi A, Roney P, Zhou Y, Zhang Z, Xiao Y, Wan C, et al. Temperature-independent thermal radiation. Proc Natl Acad Sci U S A 2019;116:26402–6. doi:10.1073/pnas.1911244116.
[18] Lyu J, Liu Z, Wu X, Li G, Fang D, Zhang X. Nanofibrous Kevlar Aerogel Films and Their Phase-Change Composites for Highly Efficient Infrared Stealth. ACS Nano 2019 acsnano.8b08913. doi:10.1021/acsnano.8b08913.
[19] Shi R, Shen N, Wang J, Wang W, Amini A, Wang N, et al. Recent advances in fabrication strategies, phase transition modulation, and advanced applications of vanadium dioxide. Appl Phys Rev 2019;6. doi:10.1063/1.5087864.
[20] Prod'homme H, Ordonez-Miranda J, Ezzahri Y, Drévillon J, Joulain K. VO2-based radiative thermal transistor with a semi-transparent base. J Quant Spectrosc Radiat Transf 2018;210:52–61. doi:10.1016/j.jqsrt.2018.02.005.
[21] Tang K, Wang X, Dong K, Li Y, Li J, Sun B, et al. A Thermal Radiation Modulation Platform by Emissivity Engineering with Graded Metal–Insulator Transition. Adv Mater 2020;32:1–6. doi:10.1002/adma.201907071.
[22] Yang Z, Ko C, Ramanathan S. Oxide electronics utilizing ultrafast metal-insulator transitions. Annu Rev Mater Res 2011;41:337–67. doi:10.1146/annurev-matsci-062910-100347.
[23] Kats MA, Blanchard R, Zhang S, Genevet P, Ko C, Ramanathan S, et al. Vanadium dioxide as a natural disordered metamaterial: perfect thermal emission and large broadband negative differential thermal emittance. Phys Rev X 2014;3:1–7. doi:10.1103/PhysRevX.3.041004.
[24] Cakir MC, Kocer H, Durna Y, Yildirim DU, Ghobadi A, Hajian H, et al. Unveiling the optical parameters of vanadium dioxide in the phase transition region: a hybrid modeling approach. RSC Adv 2020;10:29945–55. doi:10.1039/D0RA05890D.
[25] Kocer H, Ozer A, Butun S, Wang K, Wu J, Kurt H, et al. Thermally tuning infrared light scattering using planar layered thin films and space gradient metasurface. IEEE J Sel Top Quantum Electron 2019;25:1–7. doi:10.1109/JSTQE.2019.2900607.
[26] Kocer H, Butun S, Banar B, Wang K, Tongay S, Wu J, et al. Thermal tuning of infrared resonant absorbers based on hybrid gold-VO2 nanostructures. Appl Phys Lett 2015;106. doi:10.1063/1.4918938.
[27] Kocer H, Butun S, Palacios E, Liu Z, Tongay S, Fu D, et al. Intensity tunable infrared broadband absorbers based on VO 2 phase transition using planar layered thin films. Sci Rep 2015;5:1–7. doi:10.1038/srep13384.
[28] Cavalleri A, Tóth C, Siders CW, Squier JA, Ráksi F, Forget P, et al. Femtosecond structural dynamics in vo2 during an ultrafast solid-solid phase transition. Phys Rev Lett 2001;87 237401-1-237401–4. doi:10.1103/PhysRevLett.87.237401.
[29] Stefanovich G, Pergament A, Stefanovich D. Electrical switching and Mott transition in VO2. J Phys Condens Matter 2000;12:8837–45. doi:10.1088/0953-8984/12/41/310.
[30] Kim Y, Wu PC, Sokhoyan R, Mauser K, Glaudell R, Kafaie Shirmanesh G, et al. Phase Modulation with Electrically Tunable Vanadium Dioxide Phase-Change Metasurfaces. Nano Lett 2019;19:3961–8. doi:10.1021/acs.nanolett.9b01246.
[31] Hashemi MRM, Yang SH, Wang T, Sepúlveda N, Jarrahi M. Electronically-Controlled Beam-Steering through Vanadium Dioxide Metasurfaces. Sci Rep 2016;6:1–8. doi:10.1038/srep35439.
[32] Aetukuri NB, Gray AX, Drouard M, Cossale M, Gao L, Reid AH, et al. Control of the metal-insulator transition in vanadium dioxide by modifying orbital occupancy. Nat Phys 2013;9:661–6. doi:10.1038/nphys2733.
[33] Wu S-H, Chen M, Barako MT, Jankovic V, Hon PWC, Sweatlock LA, et al. Thermal homeostasis using microstructured phase-change materials: erratum. Optica 2018;5:1155. doi:10.1364/optica.5.001155.
[34] Wan C, Zhang Z, Woolf D, Hessel CM, Rensberg J, Hensley JM, et al. On the Optical Properties of Thin-Film Vanadium Dioxide from the Visible to the Far Infrared. Ann Phys 2019;531:1–7. doi:10.1002/andp.201900188.
[35] Kats MA. Thermal-emission engineering with dynamically tunable materials (Conference Presentation); 2020. doi:101117/122546739.
[36] Palik E. Handbook of optical constants of solids. Elsevier; 1998.
[37] Yeh P. Optical waves in layered media. Wiley; 2005.
[38] Byrnes S.J. Multilayer optical calculations. ArXiv:1603.02720 2016:1–20.
[39] Kats MA, Sharma D, Lin J, Genevet P, Blanchard R, Yang Z, et al. Ultra-thin perfect absorber employing a tunable phase change material. Appl Phys Lett 2012;101. doi:10.1063/1.4767646.
[40] Larciprete MC, Centini M, Paoloni S, Fratoddi I, Dereshgi SA, Tang K, et al. Adaptive tuning of infrared emission using VO2 thin films. Sci Rep 2020;10:1–10. doi:10.1038/s41598-020-68334-2.
[41] Planck M. Ueber das Gesetz der Energieverteilung im Normalspectrum. Ann Phys 1901;309:553–63. doi:10.1002/andp.19013090310.